arXiv:1606.06410v1 [cond-mat.quant-gas] 21 Jun 2016

First and second global sound velocity of a Bose gas across the transition to Bose-Einstein condensation

Amilson R. Fritsch, Pedro E. S. Tavares, Franklin A. J. Vivanco,
Gustavo D. Telles, Vanderlei S. Bagnato, and Emanuel A. L. Henn
Instituto de Física de São Carlos, Universidade de São Paulo,
Caixa Postal 369, 13560-970 São Carlos, SP, Brazil
(Dated: June 22, 2016)

We present an alternative approach for determining the sound modes in atomic Bose-Einstein condensates, based on thermodynamic global variables. The total number of trapped atoms was carefully studied as a function of temperature across the phase transition, at constant volume. It allowed us to evaluate the first and second sound independently resulting in consistent values from the quantum to classical regime, in good agreement with previous results found in the literature. We also provide some insight on the dominant mode, either thermal or superfluid, on each sound velocity depending on the temperature range.

I. INTRODUCTION

There are many striking differences between normal fluids, studied through standard hydrodynamics [1], and quantum fluids, which behavior is governed by quantum hydrodynamics [2]. Some of them, however, stand out, like the existence of two sound modes in superfluids [3] in contrast to a single, unique sound velocity in normal fluids.

The origin of two sound velocities in superfluids resides in the motion of the superfluid component as an independent degree of freedom [4, 5], eventually modeled, together with the normal component, in a two-fluid hydronamic theory [5]. This treatment has been developed and widely applied to liquid Helium and the seminal contributions are due to Tisza, Landau and Bogoliubov [5–7].

The velocity of long wavelength excitations is directly connected on how changes on the local pressure and density of the fluid are related. Indeed, as we will review later, the velocity of sound is proportional to the derivative of pressure in relation to density. In the two fluid model, since the superfluid component is treated separately from the normal component, there can be two independent modes for density perturbations: (i) the first sound, analogous to the sound velocity in normal fluids, where superfluid and normal components move in-phase, which is essentially a density wave and (ii) an out-of-phase oscillation of the components, also regarded as a temperature wave, named second-sound.

Although the theory has been developed for liquid Helium, it is not easy to experimentally investigate sound modes in this framework, since interactions are very strong. On the other hand, Bose-Einstein condensates, to which quantum hydrodynamics fully apply with spectacular results [8], are very versatile systems where the parameters, e.g. geometry, interactions, total number of particles, atomic density and temperature, can be adjusted almost at will and, most importantly, the superfluid and normal components can be directly imaged and separately treated. Indeed, in atomic superfluids, first and second sound modes take a slightly different character: at high temperatures the former is identified as an oscillation of the thermal cloud density and the latter as an oscillation of the BEC density, while close to $T = 0$ this is reverted.

The first measurements of the sound velocity in a BEC were performed by Andrews et al [9] by inducing a density perturbation in the BEC and observing its time propagation allowing a direct measurement of the excitation velocity. In order to compare their results with theory, authors treated the density as homogeneous at half the peak density of the BEC, since they would not have access to local density or pressure of the fluid. This study triggered various theoretical works [10, 11] and eventually the sound velocity was studied in optical lattices [12, 13], the excitation spectrum has been measured [14] and also shock waves were observed [15, 16].

A few years ago, Meppelink et al [17] revisited and extended the early works by observing a sound wave in the BEC at finite temperatures and with improved techniques, allowing them to produce smaller density perturbations and therefore avoid non-linear effects. The obtained results display a good agreement with the theory.

Recently, the sound modes of quantum fluids have been investigated in fermi gases [18–20], lower dimensionality [21], in the context of spin-orbit coupled BECs [22] and in the presence of disorder[23].

Here we take a different approach to investigate the first and second sound modes of a Bose gas at finite temperature across the Bose-Einstein condensation transition. In fact, in contrast to previous experimental investigations, we do not imprint a density perturbation in the BEC but instead we take a cloud in equilibrium and evaluate directly its global thermodinamic variables [24]. By varying the number of atoms in the cloud for several different temperature values, keeping the global volume parameter constant, we can evaluate the variation of the global pressure parameter with density and extract the sound velocity behavior. This thermodynamic approach allows us to compare our results with the original thermodynamic derivation of the sound velocity for a quantum

gas. Besides, we can evaluate the two sound modes separately, which, to our knowledge, is the first independent measurement of first and second sound modes of a Bose gas.

II. THEORETICAL BACKGROUND

In the following we review the basic theoretical aspects related to the evaluation of the sound velocity in ultracold clouds and how we use the global thermodynamic variables to evaluate it in this work. We restrict ourselves to key results and refer the reader to more complete and comprehensive reviews of these subjects [25, 26].

When studying small amplitude oscillations of the density of an uniform Bose gas under the condition of local thermal equilibrium, one can specify the local state of the system by its total particle density ρ, the superfluid velocity v_s, its temperature T and the velocity of the excitations of the fluid.

Upon writing the continuity equation for the density and mass current one ends up with an equation relating the density and pressure p of the fluid:

$$\frac{\partial^2 \rho}{\partial t^2} = \nabla^2 p. \tag{1}$$

Also, one can write a relation between the velocity of the superfluid and the chemical potential μ which eventually leads, after some manipulation via thermodinamic relations, to

$$\frac{\partial^2 s}{\partial t^2} = \frac{\rho_s}{\rho} s^2 \nabla^2 T, \tag{2}$$

where m is the mass of the particles, s is entropy per unit mass and ρ_s is the superfluid density. Since s depends on the density and temperature itself, one can immediately identify equations (1) and (2) as coupled equations for temperature and pressure.

Solving the coupled equation by looking for small amplitude plane wave solutions one find a quartic equation for the velocity of the excitations, which, for $\rho_s \neq 0$ has two distinct solutions, identified as the first and second sound modes of the quantum fluid.

The sound modes have rather simple expressions at very specific limits. At very low temperatures,

$$c_1^2 = \frac{\partial p}{\partial \rho} \tag{3}$$

approaching the zero temperature Bogoliubov limit

$$c_1^2 = \frac{gn}{m}, \tag{4}$$

where $g = \frac{4\pi\hbar^2 a}{m}$ with a the s-wave scattering length.

At higher temperatures with non-zero superfluid density, c_1 is composed by two terms: the first, smaller, similar to Eq. (3), taken at constant temperature, and the second dependent on the entropy of the system, the dominant one [25]. As we shall see later, we do not know how to calculate entropy for our system and, at this regime, we can only evaluate the smaller term. In any case, c_1^2 displays a linear behavior just before and across the critical temperature T_c.

If $\rho_s = 0$, there is only one solution of the sound velocity equation which recovers the usual sound velocity of a fluid

$$c^2 = \frac{\partial p}{\partial \rho}. \tag{5}$$

The second sound mode c_2, in its turn, is given for most of the temperature range by

$$c_2^2 = \frac{\rho_s}{\rho}\left(\frac{\partial p}{\partial \rho}\right)_T \approx \frac{\rho_s}{\rho} c_1^2. \tag{6}$$

This expression is valid everywhere but at the very low temperatures. It should, nevertheless, give the correct zero temperature result.

Global thermodynamic variables were recently defined by Romero-Rochín [27] as an alternative approach to treat the thermodynamics of a gas which is not confined by rigid walls but rather by a non-homogeneous trap that extends everywhere in space and interacts with the atomic distribution differently at each point. We have already successfully used this approach to investigate several thermodynamic quantities in Bose gases [28, 29].

In general, when dealing with non-homogeneous trapping potentials, the standard definitions of pressure (P) and volume (V) do not apply. Indeed, P and V are conjugate variables defined for homogeneous density distributions. In particular, P should have the same value in every position inside the volume occupied by the gas, in strong contrast to a non-uniform density distribution, where it changes from point-to-point in space. It is possible then to define the so-called global variables to describe the thermodynamics of an inhomogeneous system [30].

In brief, starting from thermodynamic and statistical mechanics assumptions we define a volume parameter and a pressure parameter, respectively:

$$\mathcal{V} = \frac{1}{\omega_x \omega_y \omega_z} \tag{7}$$

and

$$\Pi = \frac{2}{3\mathcal{V}} \langle U(\mathbf{r}) \rangle, \tag{8a}$$

$$= \frac{2}{3\mathcal{V}} \int n(\mathbf{r})(\omega_x^2 x^2 + \omega_y^2 y^2 + \omega_z^2 z^2) d^3 r, \tag{8b}$$

where ω_i are the trapping frequencies, $\langle U(\mathbf{r}) \rangle$ is the spatial mean of the external potential and $n(\mathbf{r})$ is the density distribution of the gas.

It should be noted that, since we can write and experimentally identify $n(\mathbf{r}) = n_{thermal}(\mathbf{r}) + n_{BEC}(\mathbf{r})$, we

can always write $\Pi = \Pi_{thermal} + \Pi_{BEC}$ and evaluate independently the pressure parameter of both the thermal and BEC components.

These variables have being proven to be a pair of conjugate variables, adequate to describe a non-homegeneous system and which lead to the standard P and V in the thermodynamic limit [24, 27, 31].

Under this context, we **define** a global sound mode velocity for the Bose gas as:

$$c_{1g}^2 = \frac{\partial \Pi}{\partial \rho}. \tag{9}$$

Upon writing $\rho = \frac{mN}{\mathcal{V}}$, where N is the total number of atoms each with mass m confined in a Volume $\mathcal{V}$, the Eq. (9) can be rewritten as

$$c_{1g}^2 = \frac{1}{m}\frac{\partial \Pi}{\partial(\frac{N}{\mathcal{V}})}. \tag{10}$$

If the volume is kept fixed, as it is the case in our experiment, since we do not change the trap, then

$$c_{1g}^2 = \frac{\mathcal{V}}{m}\frac{\partial \Pi}{\partial N}. \tag{11}$$

By computing the variation of Π with N in our experiment, we can immediately evaluate the first and second sound velocity modes of the cloud.

III. EXPERIMENTAL SEQUENCE

The experimental setup and procedure is thoroughly described in previous works [32, 33]. The starting point of our experiments is a sample of ^{87}Rb atoms spin-polarized in the $|F = 2, m_F = +2\rangle$ hyperfine state in a harmonic magnetic trap with trapping frequencies given by $\omega_z = 2\pi \times 21.1(1)$Hz and $\omega_r = 2\pi \times 188.2(3)$Hz. Sound velocity (Eq. (11)) is evaluated above, around and below the critical temperature T_c for Bose-Einstein condensation. Atom-number ranges from 1×10^6 at $2\,\mu$K in a fully thermal cloud to $1 - 2 \times 10^5$ Bose-condensed atoms with no distinguishable thermal component, indicating condensed fractions $N_0/N > 70\%$. After reaching a final given state, the trap is switched off and the atoms are allowed to freely expand for 23 ms, after which they are imaged through standard resonant absorption imaging. By fitting the thermal (condensed) cloud images with well-stablished gaussian (Thomas-Fermi) profiles we extract the number of condensed atoms, number of thermal atoms, typical sizes, densities and the temperature of the cloud.

The number of atoms as well as their final temperature is controlled by increasing or decreasing the initial number of atoms loaded in the trap and/or by the radio frequency used in the process of forced evaporative cooling.

For this work we run the experiment varying the number of atoms and the temperature in the widest range of combinations allowed by our experimental setup to obtain a precise measurement of the sound velocity. After this set of data is obtained, we group together images in the same temperature range within ± 5 nK.

In order to calculate the global pressure parameter Π, Eq. (8), we use the well stablished Castin-Dum regression [34] to determine the *in situ* dimensions of the cloud, its in-trap density distribution and, together with the knowledge of the trapping potential, the pressure parameter for each cloud. This is the exact same procedure we have used in several previous works [24, 28, 29] to evaluate the equation of state, the observation of a BEC, its compressibility, among other phenomena.

In Fig. 1 we show typical data for the pressure parameter obtained by the above-described procedure as a function of the number of atoms for three given temperatures. The displayed behavior is clearly linear and we extract the slope of this curve, which is the important quantity to evaluate the global sound velocity, by fitting it with a simple linear function. Tipically, we impose a minimum of 5 datapoints for each given temperature to confidently evaluate the data, but most of the datasets are much larger and comparable to what is shown in Fig. 1.

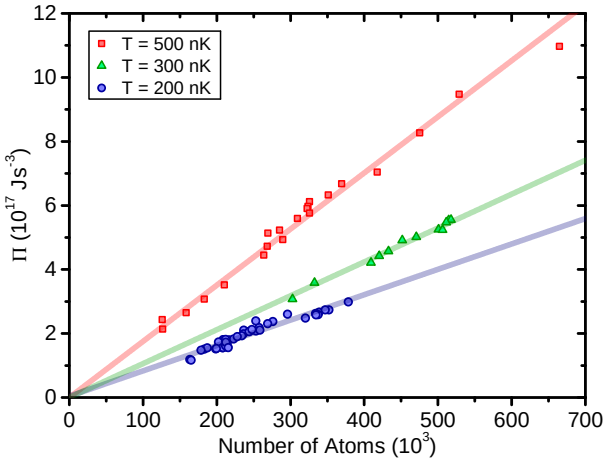

Figure 1. Typical sets of data used for calculating sound velocity. The squares are data for 500 nK, triangles are data for 300 nK and circles are the selected data in the temperature of 200 nK.

The sound velocity in our approach only depends on the slope of this plot, the mass of Rubidium atoms, and the volume parameter, which for our experiment is $\mathcal{V} = 5.4 \times 10^{-9}$ s^3 and remains the same since it only depends on the trapping frequencies.

IV. RESULTS

Figure 2 shows the squared global first sound velocity, c_{1g}^2 as defined in Eq. (9), as a function of temperature evaluated by the procedure previously described. The first feature to be noticed is that at very low tempera-

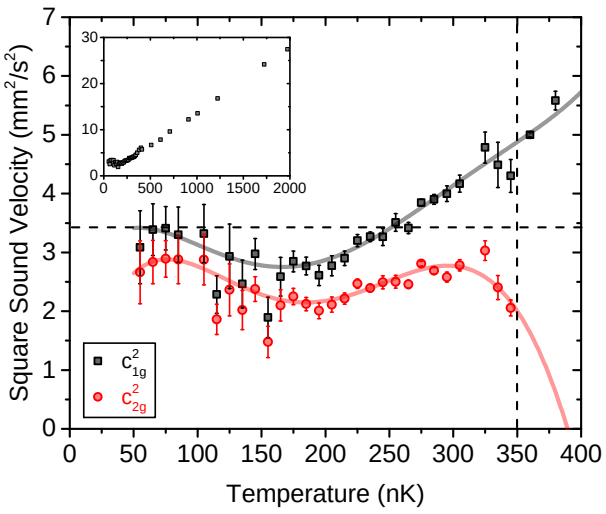

Figure 2. Squared global first (black squares) and second (red circles) sound modes of a Bose-Einstein condensate as a function of temperature. Solid lines are guides to the eye. Dashed horizontal line is the theoretical zero temperature value of c_{1g}^2 and dashed vertical line is the approximate temperature above which no superfluid fraction is detected. Inset shows a broader range of temperatures for c_{1g}^2 where one can see the expected linear behavior for higher temperatures.

tures, the first sound mode approaches its zero temperature value, Eq. (4), represented by the horizontal dashed line. Also, at higher temperatures and while $\rho_s \neq 0$, represented by the region of temperatures below the vertical dashed line, one observe the expected linear behavior of the first sound mode with temperature.

The inset of Fig. 2 displays a wider range of temperatures, well into the region where $\rho_s = 0$. First thing to notice here is that the observed behavior of the sound velocity in the thermal cloud is the expected linear growth which extrapolates to zero at $T = 0$ in the absence of a BEC transition. Moreover, the observed rate $\frac{\Delta(c_{1g}^2)}{\Delta T} = 1.3 \times 10^{-2}\,\mathrm{mm^2 s^{-2} nK^{-1}}$ is lower than the theoretical expected value $8.2 \times 10^{-2}\,\mathrm{mm^2 s^{-2} nK^{-1}}$, as it was discussed in Sec. II. Although not quantitatively precise, this also highlights an advantage of our method: one does not need to imprint density perturbations in the cloud to measure the sound velocity. Those would be very difficult to follow in a thermal cloud due to the natural damping, not allowing to measure any sound mode velocity in this regime. Our method, on its turn, allow an estimate of the quantity with $\rho_s \neq 0$, $\rho_s = 0$ and across the BEC transition.

We also evaluate the second sound mode of the cloud, displayed on Fig. 2 as red open dots, through Eq. (6). Despite not being valid in the whole range, it is, to our knowledge, the first measurement of c_{2g}^2 in a Bose gas. Nevertheless, the second sound mode shows the expected behavior, approaching zero as $T \to T_c$ and being smaller than the first sound mode value for the whole range.

Our method allows us to independently treat two other sets of quantities related to the sound velocity and that can give some additional insight on our results. The first quantities are the partial components of the first sound velocity, given by the independent derivative of the BEC and thermal pressure parameters with respect to the total number of atoms:

$$c_{BEC-part}^2 = \frac{\mathcal{V}}{m}\frac{\partial \Pi_{BEC}}{\partial N} \tag{12}$$

and

$$c_{ther-part}^2 = \frac{\mathcal{V}}{m}\frac{\partial \Pi_{ther}}{\partial N}. \tag{13}$$

One can immediately notice that our defined global first sound velocity, Eq. (9), is given by the sum of the above-defined partial components

$$c_{1g}^2 = c_{BEC-part}^2 + c_{ther-part}^2. \tag{14}$$

The second set of quantities are the independent BEC e thermal sound velocities as if they were completely independent separate fluids:

$$c_{BEC}^2 = \frac{\mathcal{V}}{m}\frac{\partial \Pi_{BEC}}{\partial N_{BEC}} \tag{15}$$

and

$$c_{ther}^2 = \frac{\mathcal{V}}{m}\frac{\partial \Pi_{ther}}{\partial N_{ther}}. \tag{16}$$

Note that

$$c_{BEC-part}^2 + c_{ther-part}^2 \neq c_{BEC}^2 + c_{ther}^2 \tag{17}$$

but still both can give valuable information as we discuss in the following.

Figure 3(a) shows the partial components of the sound velocity $c_{BEC-part}^2$ and $c_{ther-part}^2$ and Fig. 3(b) shows the independent sound velocities c_{BEC}^2 and c_{ther}^2. In both cases we plot solid lines as guides to eye that follow, respectively, the highest and lowest values of both sound modes at each temperature.

In Fig. 3(a) one can see the range where each component dominates the first sound mode: below ≈ 150 nK the BEC component dominates a vanishingly small thermal component while above it the thermal cloud dominates. This observed behavior follows closely the interpretation of the sound modes given in Ref. [26], which says that the sound mode associated to the thermal cloud is the first sound at high temperatures while at low temperatures, the first sound is given by the BEC part. Conversely, the second sound mode is identified as the BEC mode at high temperatures and the thermal mode at low temperatures.

This change of characters leads to the well-known avoided crossing in the two sound modes [10] that can be better illustrated when we compute the independent sound velocities, as shown in Fig. 3(b), and identify the larger value of them as an approximation for c_1^2 and the

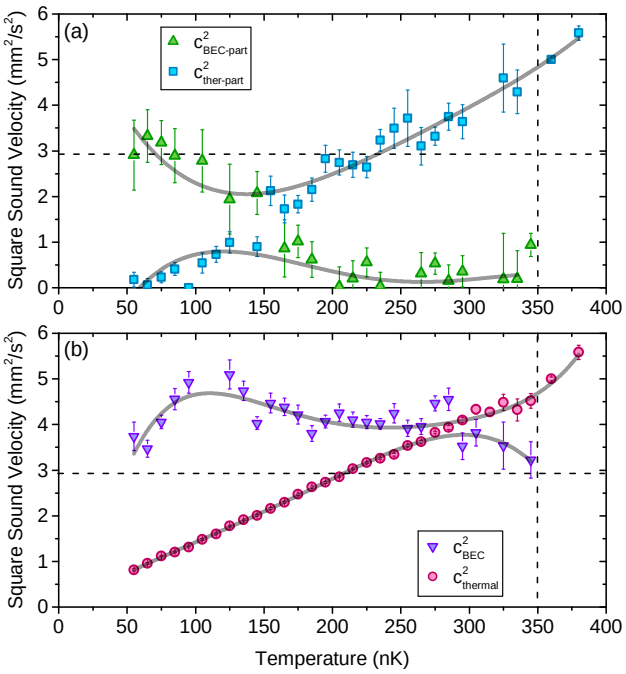

Figure 3. (a) Partial components of the first global sound velocity, given by the BEC (green up-triagles) and thermal parts (blue squares). (b) "Single fluid" (see text) sound velocity of the BEC (purple down-triangles) and thermal fluids (magenta circles). The solid lines in both (a) and (b) are guides to the eye following either the highest or lowest value of both sound modes at each temperature. The horizontal dashed line is the theoretical predicted $T = 0$ first sound velocity and the vertical dashed line is the approximate limit above which no superfluid fraction is detected at our experiments.

lower as an approximation for c_2^2. In this figure one observes the dominant mode change, the first sound, given by the BEC mode at low temperatures, approaching its $T = 0$ value, given by the horizontal dashed line, and the expected first mode linear behavior after the avoided crossing, now given by the thermal mode. Also, we can identify the second mode sound, given by the thermal component at low temperatures and the BEC component at higher temperatures, approaching its maximum value close to the avoided crossing and vanishing as $T \to 0$ and $T \to T_c$, which is the predicted behavior in several references, e.g Ref. [35]. Naturally, as we have stated before, the independent calculated sound modes c^2_{BEC} and c^2_{ther} must not be taken as the perfect representatives of the first and second sound modes, since they are not truly decoupled and the very existence of the two modes arises from a two-fluid model but, still, the observed behavior certainly matches the widespread interpretations of the modes.

Finally, from Fig. 3(b) one can also see that the thermal mode approaches zero linearly as the temperature is lowered, as expected and the BEC mode has a mean value of $c^2_{BEC} \approx 4.0\,\mathrm{mm}^2/\mathrm{s}^2$ with a low dispersion around it, slightly above the expected zero-temperature value of $\approx 3.5\,\mathrm{mm}^2/\mathrm{s}^2$.

In conclusion, we have defined and evaluated a global sound velocity of a Bose gas throughout a wide range of temperatures and across the Bose-Einstein condensation transition, allowing us to compute the first and second sound modes of the BEC. We have also shown that the BEC and thermal modes change dominance and character with respect to the two sound modes, leading to an avoided crossing in accordance with the predicted behavior by two-fluid theory. We have also shown that several qualitative and quantitative features are reproduced by our analysis.

ACKNOWLEDGMENTS

This work has been supported by Fapesp, under the program CePID, grant 2013/07276-1. A.R.F. and P.E.S.T. acknowledge CAPES scholarships and E.A.L.H. and V.S.B CNPq research fellowships.

[1] L. D. Landau and E. M. Lifshitz, *Fluid Mechanics*, Course of Theoretical Physics (Pergamon press, 1987).
[2] P. Nozières and D. Pines, *The Theory of Quantum Liquids* (Perseus Books Publishing, 1999).
[3] L. Tisza, Nature **141**, 913 (1938).
[4] F. London, Nature **141**, 643 (1938).
[5] L. Landau, Phys. Rev. **60**, 356 (1941).
[6] L. Tisza, J. Phys. Radium **1**, 164 (1940).
[7] N. Bogoliubov, J. Phys. **11**, 23 (1947).
[8] D. S. Jin, J. R. Ensher, M. R. Matthews, C. E. Wieman, and E. A. Cornell, Phys. Rev. Lett. **77**, 420 (1996); M.-O. Mewes, M. R. Andrews, N. J. van Druten, D. M. Kurn, D. S. Durfee, C. G. Townsend, and W. Ketterle, Phys. Rev. Lett. **77**, 988 (1996); D. M. Stamper-Kurn, H.-J. Miesner, S. Inouye, M. R. Andrews, and W. Ketterle, Phys. Rev. Lett. **81**, 500 (1998); O. M. Maragò, S. A. Hopkins, J. Arlt, E. Hodby, G. Hechenblaikner, and C. J. Foot, Phys. Rev. Lett. **84**, 2056 (2000).
[9] M. R. Andrews, D. M. Kurn, H.-J. Miesner, D. S. Durfee, C. G. Townsend, S. Inouye, and W. Ketterle, Phys. Rev. Lett. **79**, 553 (1997).
[10] A. Griffin and E. Zaremba, Phys. Rev. A **56**, 4839 (1997).
[11] T. Nikuni and A. Griffin, Phys. Rev. A **58**, 4044 (1998).
[12] C. Menotti, M. Krämer, A. Smerzi, L. Pitaevskii, and S. Stringari, Phys. Rev. A **70**, 023609 (2004).
[13] P. T. Ernst, S. Götze, J. S. Krauser, K. Pyka, D.-S. Lühmann, D. Pfannkuche, and K. Sengstock, Nature Physics **6**, 56 (2010).
[14] J. Steinhauer, R. Ozeri, N. Katz, and N. Davidson, Phys. Rev. Lett. **88**, 120407 (2002).
[15] B. Damski, Phys. Rev. A **69**, 043610 (2004).
[16] T. P. Simula, P. Engels, I. Coddington, V. Schweikhard, E. A. Cornell, and R. J. Ballagh, Phys. Rev. Lett. **94**, 080404 (2005).

[17] R. Meppelink, S. B. Koller, and P. van der Straten, Phys. Rev. A **80**, 043605 (2009).

[18] E. Taylor, H. Hu, X.-J. Liu, L. P. Pitaevskii, A. Griffin, and S. Stringari, Phys. Rev. A **80**, 053601 (2009).

[19] J. Joseph, B. Clancy, L. Luo, J. Kinast, A. Turlapov, and J. E. Thomas, Phys. Rev. Lett. **98**, 170401 (2007).

[20] L. A. Sidorenkov, M. K. Tey, R. Grimm, Y.-H. Hou, L. Pitaevskii, and S. Stringari, Nature **498**, 78 (2013).

[21] L. Yun-Wen and C. Ji-Sheng, Communications in Theoretical Physics **60**, 673 (2013).

[22] W. Zheng and Z. B. Li, Phys. Rev. A **85**, 053607 (2012).

[23] C. Gaul, N. Renner, and C. A. Müller, Phys. Rev. A **80**, 053620 (2009).

[24] V. Romero-Rochin, R. F. Shiozaki, M. Caracanhas, E. A. L. Henn, K. M. F. Magalhães, G. Roati, and V. S. Bagnato, Phys. Rev. A **85**, 023632 (2012).

[25] L. P. Pitaevskii and S. Stringari, *Bose-Einstein condensation* (Oxford University Press, Oxford, 2003) p. 382.

[26] C. J. Pethick and H. Smith, *Bose-Einstein condensation in dilute gases*, 1991 (Cambridge University Press, 2nd ed. Cambridge, 2008) p. 569.

[27] V. Romero-Rochín, Phys. Rev. Lett. **94**, 130601 (2005).

[28] R. F. Shiozaki, G. D. Telles, P. Castilho, F. J. Poveda-Cuevas, S. R. Muniz, G. Roati, V. Romero-Rochin, and V. S. Bagnato, Phys. Rev. A **90**, 043640 (2014).

[29] F. J. Poveda-Cuevas, P. C. M. Castilho, E. D. Mercado-Gutierrez, A. R. Fritsch, S. R. Muniz, E. Lucioni, G. Roati, and V. S. Bagnato, Phys. Rev. A **92**, 013638 (2015).

[30] V. Romero-Rochín and V. S. Bagnato, Brazilian Journal of Physics **35**, 607 (2005).

[31] R. R. Silva, E. A. L. Henn, K. M. F. Magalhães, L. G. Marcassa, V. Romero-Rochin, and V. S. Bagnato, Laser Physics **16**, 687 (2006).

[32] E. A. L. Henn, J. A. Seman, G. Roati, K. M. F. Magalhães, and V. S. Bagnato, Phys. Rev. Lett. **103**, 045301 (2009).

[33] E. A. L. Henn, J. A. Seman, G. B. Seco, E. P. Olimpio, P. Castilho, G. Roati, D. V. Magalhães, K. M. F. Magalhães, and V. S. Bagnato, Brazilian Journal of Physics **38**, 279 (2008).

[34] Y. Castin and R. Dum, Phys. Rev. Lett. **77**, 5315 (1996).

[35] E. Zaremba, A. Griffin, and T. Nikuni, Phys. Rev. A **57**, 4695 (1998).